Available online at www.sciencedirect.com

SciVerse ScienceDirect

Russian Geology and Geophysics 54 (2013) 166–180

RUSSIAN GEOLOGY AND GEOPHYSICS

www.elsevier.com/locate/rgg

The Talazhin plagiodunite–troctolite–anorthosite–gabbro massif (*East Sayan*): petrogeochemistry and ore potential

A.N. Yurichev [a,*], A.I. Chernyshov[a], A.E. Konnikov[b,†]

[a] *Tomsk State University, pr. Lenina 36, Tomsk, 634050, Russia*
[b] *Institute of Experimental Mineralogy, Russian Academy of Sciences, ul. Akademika Osip'yana 4, Chernogolovka, Moscow Region, 142432, Russia*

Received 22 February 2012; accepted 21 June 2012

Abstract

The petrology and ore potential of the Talazhin massif located in northwestern East Sayan are studied. The internal structure of the intrusion, the petrographic composition of its rocks, and their metallogenic, petrostructural, and petrogeochemical features are considered. The probable temperature and chemical composition of the parental magma of the pluton were computed using the KOMAGMAT-3.52 program on the modeling of equilibrium crystallization. The obtained data indicate that the Talazhin massif is a rhythmically layered plagiodunite–troctolite–anorthosite–gabbro intrusion formed from low-Ti high-alumina olivine–basalt melt. It is promising for Cu–Ni–PGE mineralization.

Keywords: layered massifs; plagiodunites; troctolites; petrology; ore mineralization

Introduction

Intrusions of ultrabasic and basic rocks are widespread within the Kan block, East Sayan (Chernyshov et al., 2010; Kornev et al., 2003). They are united into four complexes: Idar dunite–harzburgite complex of tentatively Late Archean age; Kingash Ni-bearing dunite–wehrlite–picrite complex of Late Archean to Late Proterozoic age (according to different authors); Kulibin peridotite–pyroxenite–gabbro complex of Early Proterozoic age; and Talazhin layered plagiodunite–troctolite–anorthosite–gabbro complex of Riphean(?) age. The massifs of the Kingash complex have been investigated most comprehensively because they bear commercial Cu–Ni–PGE sulfide mineralization (Glazunov et al., 2003). The rest complexes are poorly studied. In this paper we consider the Talazhin pluton, a petrotype of the Talazhin intrusive complex. It is located in the northwest of the Kan block, within the Kirel' area, on the extension of the Kingash ore district. Study of reference objects is of great importance for geological mapping and formation analysis; therefore, we performed a complex petrological investigation of the Talazhin massif and estimated its metallogenic specialization.

The geologic structure of the Kirel' area

The Kirel' area is part of the Sayan PGE–Ni-bearing province (Glazunov, 1995) (Fig. 1). In the northeast, it is separated by the Kan–Agul' Deep Fault from the Vendian–Cambrian strata of the Kingash terrane, Devonian deposits of the Rybnaya basin, and Jurassic coaliferous sediments of the Sayan–Partizan trough. The distribution pattern of the magnetic field shows that all these deposits overlie the metamorphic rocks of the sagged Kan block (oral report by A.N. Smagin and A.V. Renzhin). In the southwest, the Kirel' area is separated by the Main East Sayan and Mana Deep Faults from the Upper Riphean volcanosedimentary and Vendian–Cambrian terrigenous-carbonate deposits of the Mana trough.

Two structural blocks of rank 2 (terranes) are recognized in the internal structure of the Kirel' area: Early Proterozoic(?) Kirel', composed mainly of metamorphosed volcanosedimentary deposits, and Late Riphean Talazhin, made up mainly of intrusive rocks. The latter block is 60×22 km^2 in area; it lies in the southwestern part of the Kirel' area, in the interfluve of the Kirel' and Mana Rivers. Ultrabasic and basic rocks amount to 80% of intrusive deposits of the block, and the rest are predominantly granitoids (Fig. 1). This is the only structure with intense intrusive magmatism within the Kan block.

* Corresponding author.
E-mail address: juratur@sibmail.ru (A.N. Yurichev)
† Deceased.

1068-7971/$ - see front matter © 2013, V.S. Sobolev IGM, Siberian Branch of the RAS. Published by Elsevier B.V. All rights reserved.
http://dx.doi.org/10.1016/j.rgg.2013.01.004

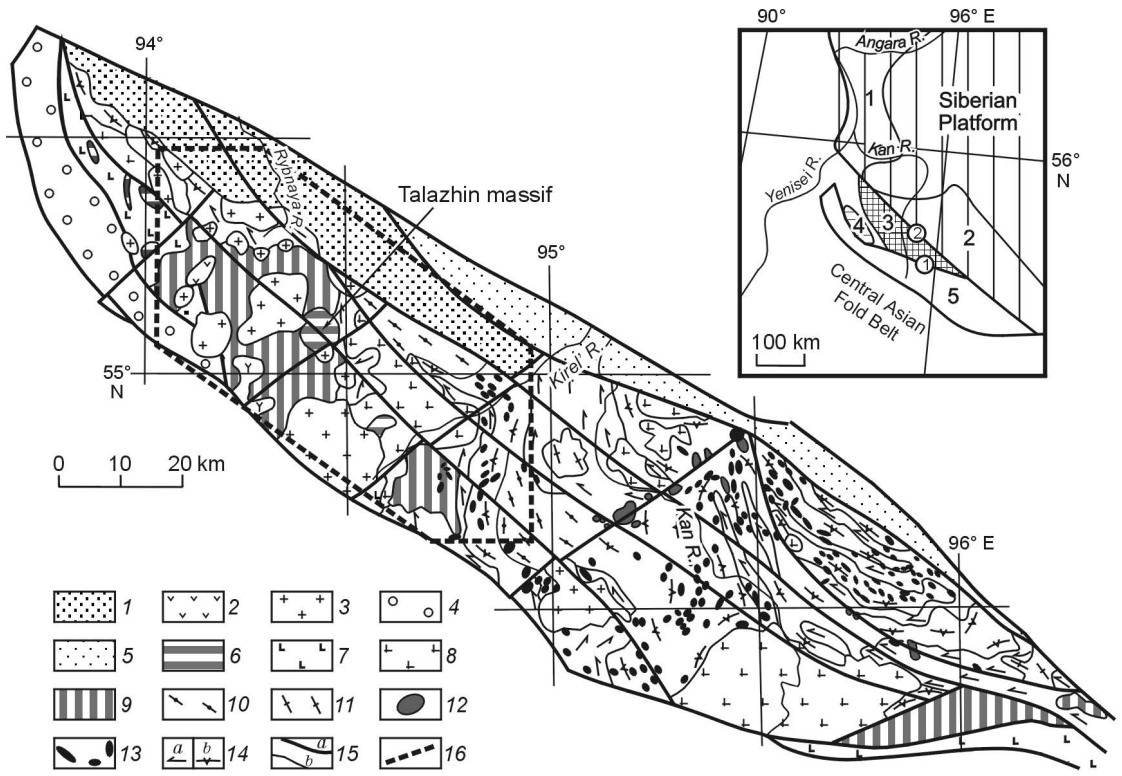

Fig. 1. Schematic geologic structure of the Kan Block (compiled after data of A.N. Smagin, A.G. Ekhanin, A.D. Nozhkin, O.M. Turkina, and A.I. Chernyshov). *1*, Upper Paleozoic–Mesozoic mainly terrigenous deposits: Karymovo, Pavlovsk, and Kungus Formations; *2*, Lower Devonian (probably, partly Ordovician) volcanics; *3*, Ordovician leucogranite formation: Kuturchin complex; *4*, Cambrian–Ordovician red-colored terrigenous deposits of the Badzhei trough; *5*, Vendian–Lower Cambrian terrigenous-carbonate deposits; *6*, Middle–Upper Riphean Talazhin plagiodunite–troctolite–anorthosite–gabbro complex; *7*, Middle–Upper Riphean volcanosedimentary rocks of the Kuvai Group; *8*, Late Riphean Kan granitoid complex; *9*, Early Proterozoic–Middle Riphean(?) peridotite–pyroxenite–gabbro formation: Kulibino complex; *10*, Early Proterozoic amphibolite–gneiss strata of the Anzha structure–material complex; *11*, Early Proterozoic Tuksha migmatite–plagiogranite complex; *12*, Late Archean (probably Early and even Late Proterozoic) Kingash dunite–wehrlite–picrite complex of small layered differentiated massifs; *13*, Late Archean–Early Proterozoic(?) Idar dunite–harzburgite complex (stocks, dikes, lenses, and sills) (some bodies have not been studied yet; they might belong to the Kingash complex); *14*, Upper Archean(?) amphibolite (*a*) and gneiss (*b*) strata of the Karagan complex; *15*, NW- and NE-striking deep faults (*a*) and geologic boundaries (*b*); *16*, boundary of the Kirel' area. Inset shows the position of the Kan block within the structures on the southwestern framing of the Siberian Platform. Salients of the crystalline platform basement: 1, Angara–Kan; 2, near-Sayan. Precambrian structures of the folded framing (blocks): 3, Kan; 4, Arzybei; 5, Derbina. Encircled figures mark faults: 1, Main East Sayan; 2, Kan–Agul'.

The internal structure of the Talazhin intrusion

The Talazhin massif was first recognized in this area by A.N. Smagin during a geological survey (1 : 50,000 scale) in the 1960–1980s and was assigned to the plagiodunite–troctolite–anorthosite–gabbro formation ($Є_3$). In 2000, the Talazhin massif was included into the Lower Derbina complex (R_3) on State Geological Map 1000/2.

The massif is rounded on the day surface (6×7.5 km^2). It is composed mainly of plagiodunites and troctolites and subordinate olivine gabbro and anorthosites. Four alternation megarhythms are recognized in its section (from Smagin's data). The thickness of rock intercalates in the megarhythms varies from 2 to 70 m (Fig. 2). In the southeast, the massif bottom dips at 30º–40º and makes contact with a unit of stratified amphibolites, calciphyrs, and marbles.

Lowest megarhythm I is 400–450 m thick and is composed of troctolites with intercalates and lenses of plagiodunites (up to 50–70 m thick) and, sometimes, anorthosites (up to 1 m thick). Troctolites, plagiodunites, and anorthosites in the megarhythm amount to 55–70, 20–35, and 10%, respectively. Plagiodunite intercalates are observed in the lower part of the megarhythm, and anorthosite intercalates, in the upper part.

Megarhythm II is made up mainly of plagiodunites and apodunite serpentinites 350–400 m thick. Plagiodunites contain intercalates of troctolites and anorthosites (up to 5–15 m thick), amounting to 20–35%.

Megarhythm III is formed mainly by troctolites (250–350 m thick) with intercalates and lenses (up to 3–20 m thick) of anorthosites (~10%), dunites and plagiodunites (20–30%), and rare thin intercalates of olivine gabbro.

Megarhythm IV completes the visible section. It is of essentially plagiodunite composition and is ~200 m thick. At the contact with megarhythm III, there is a thin alternation of plagiodunites, troctolites, and anorthosites.

The internal structure of the massif rocks points to their crystallization from magmatic melt corresponding in composition to olivine–plagioclase cotectic melt. This makes it

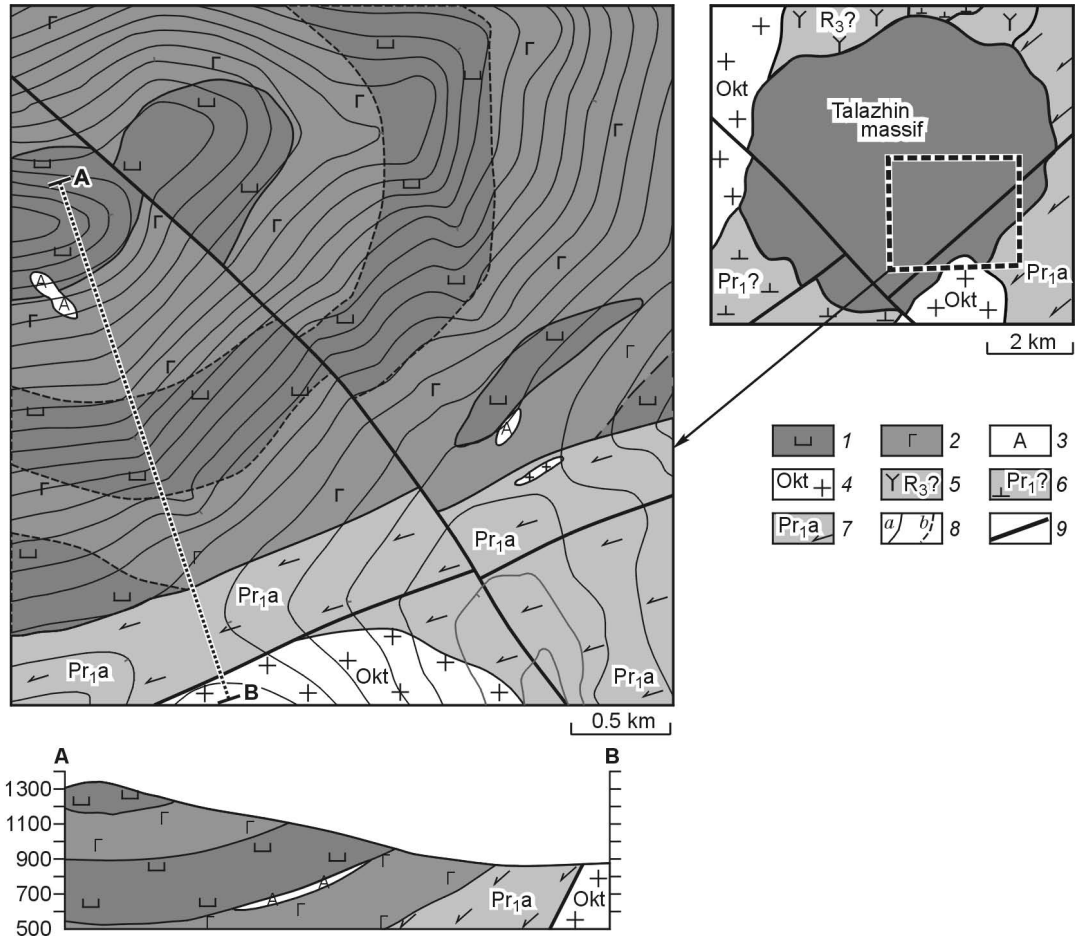

Fig. 2. Geologic scheme and geologic section of the Talazhin massif (compiled after data of A.N. Smagin and A.V. Renzhin). *1–3*, Late Riphean Talazhin layered plagiodunite–troctolite–anorthosite–gabbro complex: *1*, plagiodunites, serpentinized plagiodunites, and apodunite serpentinites, *2*, troctolites and metatroctolites with rare intercalates of olivine gabbro, *3*, intercalates and lenses of anorthosites; *4*, Ordovician Kuturchin complex; *5*, Late Riphean(?) gabbro–syenite formation; *6*, Early Proterozoic(?) peridotite–pyroxenite–gabbro formation; *7*, Early Proterozoic amphibolite strata; *8*, geologic boundaries: *a*, interpreted, partly attested, *b*, predicted from results of lithochemical survey; *9*, faults.

similar to the layered series of the Late Riphean Yoko-Dovyren pluton located in the Synnyr rift structure in the northern Baikal area (Ariskin et al., 2003, 2009; Kislov, 1998; Konnikov, 1986). In contrast to the Yoko-Dovyren pluton, the layered series of the Talazhin massif lacks an upper gabbro and gabbronorite part, which might have been destroyed by erosion. Moreover, the Yoko-Dovyren massif is underlain by a horizon of phlogopite-bearing plagiolherzolites and picrite-dolerites containing Cu–Ni sulfide mineralization.

The Talazhin massif is similar to the Late Proterozoic Voices Bay intrusion (1334 Ma) in the Labrador province, Canada, which encloses the large Voices Bay Cu–Ni deposit (Naldrett, 2003). The massif is a lopolith-like body with a bottom subsiding eastward at 25º. It is composed of troctolites grading into olivine gabbro upsection. In the near-bottom zone, troctolites are of taxitic structure. With depth, they pass into a narrow dike conduit composed of “leopard” troctolites and magmatic breccias with ultrabasic clastics (plagiodunites and plagioperidotites). The near-bottom zone is ore-bearing and encloses disseminated and massive sulfide ores.

Petrographic characteristics of intrusive rocks

Plagiodunites are medium- and coarse-grained (3–8 mm) rocks with a cumulative texture (Fig. 3*a*) and a massive structure. Locally, a kelyphitic texture is observed, which forms when kelyphite borders appear along the boundaries between olivine and plagioclase of tremolite or chlorite. Plagiodunites contain 80–90% chrysolite (18–20% Fa, Table 1) and 5–10% basic plagioclase (bytownite 76–77% An, Table 2). Accessory minerals (up to 5%) are Cr-spinels present as inclusions in olivine and in plagioclase as well as ultrarare grains of sulfides (pyrrhotite, pentlandite). Olivine crystallizes as subeuhedral, sometimes subhedral grains cut by looped cracks filled with lizardite and magnetite. There are also impurities of NiO (0.08–0.28 wt.%) and CaO (0.04 wt.%) (Table 1). Plagioclase forms fine xenomorphic aggregates of grains filling interstices between olivine crystals. Microprobe analysis also revealed impurities of FeO (0.24–0.27 wt.%) and K_2O (0.06 wt.%, Table 2).

Cr-spinels are of two varieties: dark greenish-brown and light green transparent. The first variety is euhedral grains up

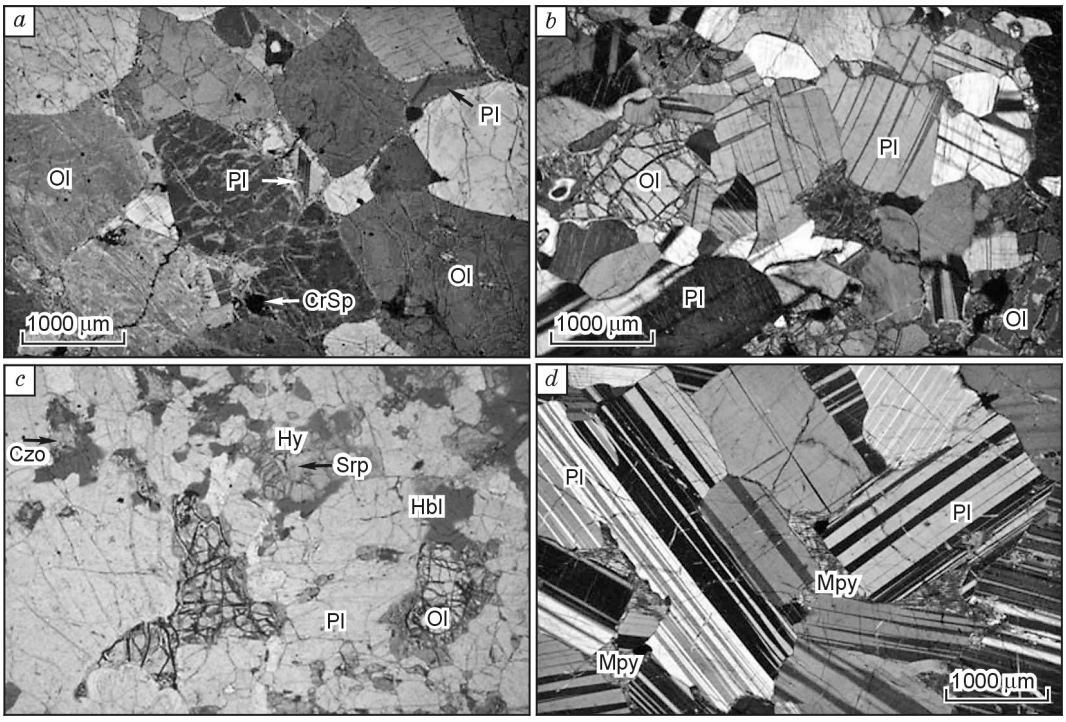

Fig. 3. Main types of rocks of the Talazhin massif. *a*, Plagiodunite; *b*, troctolite; *c*, olivine gabbro; *d*, anorthosite. Ol, olivine; Cpx, clinopyroxene; Hy, hypersthene; Hbl, hornblende; Mpy, monoclinic pyroxene; Srp, serpentine; CrSp, Cr-spinel; Czo, clinozoicite; Pl, plagioclase.

to 1 mm in size, usually replaced by magnetite (sometimes, in assemblage with ilmenite) on the periphery (Fig. 4*a*). The Cr-spinel grains show a concentric zoning: Ferroferrichromite in the core grades into ferrichromopicotite on the periphery (Table 3). The second variety (hercynites?) occurs as grains of irregular shape or their aggregates only in the interstices between olivine grains.

Sulfides were found only in weakly altered varieties of dunites; these are predominant Fe-pentlandite and subordinate troilite. They occur as rounded grains up to 0.2 mm in size. Sulfide dissemination is usually in paragenesis with Cr-spinels (Fig. 4*d*).

Plagiodunites are often subject to intense serpentinization, up to their total replacement by lizardite–antigorite and antigorite serpentinites.

Troctolites are fine- to coarse-grained (1–7 mm), sometimes porphyritic rocks composed of olivine (20–70%), plagioclase (25–70%), hypersthene (up to 5%), and hornblende (up to 10%). Sometimes clinopyroxene and biotite occur. The accessory minerals are greenish-brown spinel with magnetite borders. The rocks are of subhedral to gabbro (in places, coronated or kelyphitic) texture and massive, sometimes trachytoid structure. The secondary minerals are tremolite, talc, clinozoicite, scapolite, chlorite, and sericite.

Table 1. Chemical composition of olivine from plagiodunites, troctolites, and olivine gabbro of the Talazhin massif

Component	Plagiodunites					Troctolites					Olivine gabbro	
	1093-2	1093-3	5014/6-2	1092-4	1092-5	5014/7-2	5014-1	5014-2	5011-1	5011-2	5003/1-5	5003/1-6
SiO_2, wt.%	38.73	38.60	38.78	39.49	38.57	39.00	39.48	39.76	39.67	39.98	39.46	39.38
MgO	42.62	42.06	42.59	43.12	43.11	42.25	43.75	44.34	44.25	44.54	43.51	43.05
MnO	0.36	0.40	N.f.	0.23	0.36	0.21	0.23	0.21	0.23	0.20	0.27	0.30
FeO_{tot}	18.06	18.66	17.98	17.06	17.67	17.85	16.20	15.44	15.77	15.30	16.51	17.08
CaO	N.f.	N.f.	N.f.	N.f.	N.f.	0.04	0.03	N.f.	N.f.	0.06	N.f.	N.f.
NiO	0.13	0.28	0.08	0.13	N.f.	0.18	0.17	0.12	0.21	0.21	0.14	0.12
Total	99.9	100	99.43	100.02	99.71	99.53	99.87	99.87	100.13	100.28	99.89	99.94
Fa, mol.%	19.6	20.3	19.2	18.2	19.1	19.5	17.6	16.6	17.0	16.5	17.9	18.6

Note. Hereafter, the chemical composition of minerals was determined with a Tescan Vega II XMU scanning electron microprobe equipped with an INCA Energy 450 energy dispersion spectrometer (with a Si(Li) INCA x-sight semiconductor detector) and an INCA Wave 700 wave-dispersion spectrometer at the Institute of Experimental Mineralogy, Chernogolovka (analyst A.N. Nekrasov). N.f., Not found. Fa, Content of fayalite molecule, [F = Fe/(Fe + Mg)100].

Table 2. Chemical composition of plagioclase from the main types of rocks of the Talazhin massif

Component	Plagiodunite		Troctolites				Olivine gabbro		Anorthosites			
	5014/7-7	5014/7-8	5014-4	5014-5	5011-4	5011-5	5003/1-9	5003/1-11	5020/2-3	5015/1-6	5015/1-2	5015/1-3
SiO_2, wt.%	48.01	48.88	47.97	47.95	47.27	47.16	47.40	48.12	49.12	44.42	42.29	41.06
TiO_2	N.f.	0.06	N.f.	0.05	0.05	N.f.	0.06	0.06	0.07	0.10	0.06	0.06
Al_2O_3	32.61	32.99	32.15	32.90	32.73	33.38	31.66	33.08	32.62	31.93	32.92	33.43
FeO_{tot}	0.24	0.27	0.48	0.56	0.26	0.18	0.78	0.21	0.26	0.55	0.55	0.56
MgO	0.04	N.f.	0.10	0.07	0.05	0.05	0.37	0.05	0.06	0.10	0.11	0.11
CaO	15.55	15.37	16.52	15.52	16.78	16.25	18.06	15.81	14.91	21.15	23.05	24.66
Na_2O	2.51	2.67	1.98	2.53	2.14	2.16	1.58	2.37	2.91	1.53	0.66	0.07
K_2O	0.06	0.06	0.39	0.06	0.03	N.f.	0.25	0.08	0.05	N.f.	N.f.	N.f.
Total	99.02	100.31	99.59	99.63	99.31	99.19	100.16	99.77	100	99.77	99.64	99.94
An, mol.%	77.1	75.8	80.4	77.0	81.1	80.6	85.1	78.3	73.7	88.4	95.0	99.4

Note. An, Content of anorthite molecule, [An = Ca/(Ca + Na + K) · 100].

Olivine (Fig. 3*b*) is present as rounded, sometimes columnar subeuhedral crystals oriented in the same direction (directive structure). In composition it corresponds to chrysolite (16.5–17.5% Fa), as in the overlying plagiodunites. Olivine has impurities of NiO (0.12–0.21 wt.%) and CaO (0.03–0.06 wt.%). Olivine is usually subject to loop-shaped serpentinization. Under more intense alterations, olivine is replaced by iddingsite, talc, and tremolite. Olivine shows irregular extinction and bands of plastic fracture.

Plagioclase is usually younger than olivine and occurs as xenomorphic grains in the interstices between olivine crystals and as prismatic and tabular porphyritic phenocrysts up to 8 mm in size. In composition plagioclase corresponds to bytownite (77–81% An, Table 2). During secondary altera-

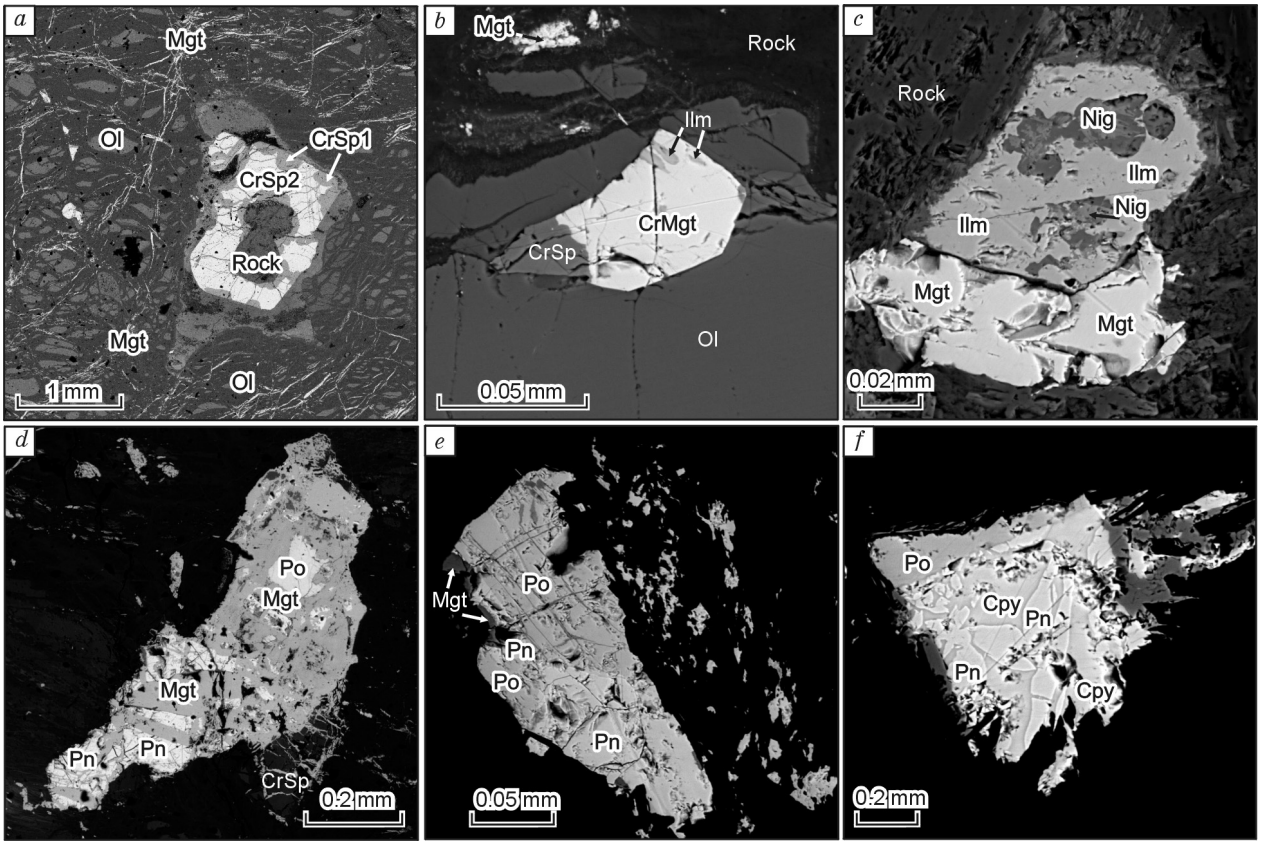

Fig. 4. Ore mineralization of rocks of the Talazhin massif. *a–f*, Description is in the text. Mgt (CrMgt), magnetite (Cr-magnetite); CrSp, Cr-spinel; Ilm, Ilmenite; Nig, nigrine; Po, pyrrhotite; Pn, pentlandite; Cpy, chalcopyrite; Ol, olivine; Rock, rock-forming silicate minerals.

Table 3. Chemical composition of Cr-spinels from plagiodunites of the Talazhin massif

Component	Picotite						Ferrichromopicotite						Ferroferrichromite					
	1093	1093	5014/6	5014/6	1092	1092	1093	1093	5014/6	5014/6	1092	1092	1093	1093	5014/6	1092	1092	1092
MgO, wt.%	15.03	16.02	16.88	16.86	17.13	16.93	11.22	10.11	6.13	10.65	8.92	6.75	1.98	2.53	1.80	0.96	0.95	1.28
Al_2O_3	65.44	65.31	65.47	65.58	65.55	65.18	38.41	34.90	28.53	43.23	38.68	36.26	4.71	4.13	4.32	3.89	5.03	6.57
CaO	N.f.	N.f.	N.f.	0.17	N.f.	N.f.	N.f.	N.f.	N.f.	N.f.	N.f.	N.f.	N.f.	N.f.	N.f.	N.f.	N.f.	N.f.
TiO_2	N.f.	N.f.	N.f.	N.f.	N.f.	N.f.	0.39	0.32	1.34	0.63	N.f.	N.f.	4.76	5.45	4.40	2.07	0.84	0.70
V_2O_5	N.f.	N.f.	N.f.	N.f.	N.f.	N.f.	N.f.	0.34	0.58	N.f.	N.f.	N.f.	0.72	0.58	1.06	1.07	N.f.	N.f.
Cr_2O_3	N.f.	N.f.	N.f.	N.f.	N.f.	N.f.	21.45	23.58	29.42	18.42	22.06	26.78	17.73	17.81	17.65	15.67	23.24	22.89
MnO	0.12	0.10	N.f.	N.f.	N.f.	N.f.	N.f.	N.f.	N.f.	N.f.	N.f.	0.67	0.73	0.82	N.f.	N.f.	N.f.	N.f.
FeO_{tot}	18.56	17.90	17.91	18.05	16.66	17.81	28.36	30.53	34.06	26.84	30.45	30.22	70.27	68.73	71.03	75.06	69.44	68.12
CoO	N.f.	N.f.	N.f.	N.f.	N.f.	N.f.	N.f.	N.f.	N.f.	N.f.	N.f.	N.f.	N.f.	N.f.	N.f.	N.f.	N.f.	N.f.
NiO	0.21	0.26	N.f.	N.f.	N.f.	N.f.	N.f.	N.f.	N.f.	N.f.	N.f.	N.f.	N.f.	N.f.	N.f.	0.70	0.54	N.f.
ZnO	N.f.	N.f.	N.f.	N.f.	N.f.	N.f.	N.f.	N.f.	N.f.	N.f.	N.f.	N.f.	N.f.	N.f.	N.f.	N.f.	N.f.	N.f.
Total	99.36	99.59	100.26	100.66	99.34	99.92	99.83	99.77	100.06	99.78	100.11	100.68	100.90	100.05	100.26	99.42	100.03	99.56
Fe_2TiO_4, %	N.f.	N.f.	N.f.	N.f.	N.f.	N.f.	0.8	0.7	3.2	1.3	N.f.	N.f.	12.6	14.5	11.8	5.6	2.2	1.9
$NiFe_2O_4$	0.4	0.5	N.f.	N.f.	N.f.	N.f.	N.f.	N.f.	N.f.	N.f.	N.f.	N.f.	N.f.	N.f.	N.f.	2.0	1.5	N.f.
$MnAl_2O_4$	0.3	0.2	N.f.	N.f.	N.f.	N.f.	N.f.	N.f.	N.f.	N.f.	N.f.	1.7	2.2	2.5	N.f.	N.f.	N.f.	N.f.
$ZnAl_2O_4$	N.f.	N.f.	N.f.	N.f.	N.f.	N.f.	N.f.	N.f.	N.f.	N.f.	N.f.	N.f.	N.f.	N.f.	N.f.	N.f.	N.f.	N.f.
$MgAl_2O_4$	59.2	61.7	64.3	64.1	65.6	64.7	48.8	44.9	28.7	45.7	39.1	30.2	7.5	6.1	9.0	5.2	5.0	6.8
$MgFe_2O_4$	N.f.	N.f.	N.f.	N.f.	N.f.	N.f.	N.f.	N.f.	N.f.	N.f.	N.f.	N.f.	2.8	7.2	0.4	N.f.	N.f.	N.f.
$FeAl_2O_4$	40.1	37.6	34.4	34.6	33.7	33.8	17.2	16.4	24.1	27.6	28.1	32.3	N.f.	N.f.	N.f.	3.0	5.5	6.8
$MnFe_2O_4$	N.f.	N.f.	N.f.	N.f.	N.f.	N.f.	N.f.	N.f.	N.f.	N.f.	N.f.	N.f.	N.f.	N.f.	N.f.	N.f.	N.f.	N.f.
$ZnFe_2O_4$	N.f.	N.f.	N.f.	N.f.	N.f.	N.f.	N.f.	N.f.	N.f.	N.f.	N.f.	N.f.	N.f.	N.f.	N.f.	N.f.	N.f.	N.f.
$FeCr_2O_4$	N.f.	N.f.	N.f.	N.f.	N.f.	N.f.	24.7	27.8	36.5	21.0	25.7	31.8	24.6	24.8	24.8	22.4	32.4	31.9
$FeFe_2O_4$	N.f.	N.f.	1.3	1.3	0.7	1.5	8.5	10.2	7.5	4.4	7.1	4.0	50.3	44.9	54.0	61.8	53.4	52.6

Note. Classification of Cr-spinels after G.A. Sokolov (1948).

tions, plagioclase is replaced by a saussurite aggregate. At the sites with a kelyphitic texture, tremolite and chlorite rims develop along the plagioclase-olivine boundaries, as in plagiodunites.

Hypersthene usually occurs as borders on olivine and exhibits pink-tint pleochroism. The interstices sometimes contain colorless xenomorphic grains of clinopyroxene with cleavage at 87°, which are often overgrown with rims of brown hornblende corresponding, according to the classification by Leake et al. (1997), to magnesian and tschermakite varieties (Table 4). Hornblende also grows over olivine or hypersthene grains. Sometimes flakes of brown biotite occur.

Troctolites often bear fine (≤0.25 mm) disseminated magnetite–ilmenite–Cr-spinel (Fig. 4*b*) and pyrrhotite–pentlandite–chalcopyrite (Fig. 4*e*) mineralization. The revealed sulfides often contain a gold impurity (up to 0.36%).

Olivine gabbro is of fine-grained gabbro texture and massive structure and has the following mineral composition: plagioclase—40–50%, olivine—30–40%, and clinopyroxene—20%. The secondary minerals are chlorite, sericite, and ore minerals (Fig. 3*c*). Olivine and plagioclase occur as euhedral grains. Plagioclase sometimes has tabular polysynthetic twinned crystals. It is weakly altered (sometimes, slightly sericitized). According to chemical composition, plagioclase is bytownite (78–85% An). Olivine contains impurities of NiO (up to 0.12–0.14 wt.%) and CaO (up to 0.06 wt.%). It also includes 18–19% Fa. The mineral is subjected to secondary alterations, such as looped lizarditization and formation of secondary dust-like magnetite. The clinopyroxene grains are more xenomorphic than the olivine and plagioclase grains, are of light lilac tints, and are characterized by a large angle of extinction (up to 40°). The olivine gabbro bears fine grains of ore minerals (≤0.5 mm) similar to those in the troctolites (Fig. 4*f*).

Anorthosites are fine- to medium-grained (1–4 mm) rocks with a paneuhedral texture (and, if xenomorphic clinopyroxene is present, with a subeuhedral texture) and a massive structure. They are composed mostly (90–100%) of plagioclase (bytownite—74–88% An, anorthite—95–99% An, Table 2) and subordinate (~10%) clinopyroxene. The secondary minerals are tremolite, chlorite, clinozoicite, calcite, and sericite.

Table 4. Chemical composition of hornblende from gabbroids of the Talazhin massif

Component	Troctolites		Olivine gabbro		
	5003/5-2	5003/5-3	5003/1-1	5003/1-2	5003/1-10
SiO_2, wt.%	41.69	45.12	42.24	41.13	43.12
MgO	12.36	15.95	14.97	14.15	16.26
Al_2O_3	16.80	14.91	11.16	12.20	13.03
MnO	0.18	0.15	0.14	0.11	0.09
FeO_{tot}	13.67	7.80	10.54	10.05	7.35
CaO	9.43	11.45	11.62	11.50	11.79
Na_2O	2.59	2.09	2.27	2.52	2.47
K_2O	0.15	0.13	1.12	1.02	0.59
TiO_2	0.13	0.08	3.31	4.99	2.62
Cr_2O_3	–	–	0.18	0.14	0.22
H_2O	2.00	2.00	2.00	2.00	2.00
Total	99.00	99.67	99.54	99.81	99.54
f	38.30	21.52	28.32	28.49	20.22

Note. *f*, Fe/(Mg + Fe) · 100%.

Plagioclase crystallized as subeuhedral tabular grains 1.5–3 mm in size (Fig. 3*d*). It is replaced (sometimes, completely) by sericite or saussurite. Clinopyroxene fills the interstices between plagioclase crystals and is often replaced by secondary chlorite and tremolite. Anorthosites bear disseminated fine (≤0.25 mm), often intergrown magnetite–ilmenite grains (Fig. 4*c*). Sulfide mineralization has not been detected.

Results of petrostructural studies of olivine

Petrostructural analysis makes it possible to elucidate the mechanisms and sequence of crystallization and plastic deformations of minerals in igneous rocks. Olivine in magmatic melt is oriented predominantly along the grain elongation and reflects the effect of magma flow.

Petrostructural studies of olivine were carried out in disoriented samples of plagiodunite and troctolite; therefore, the obtained petrostructural patterns have no spatial orientation. The main problem of interpretation of these patterns is to establish the spatial correlation between the orientation of the optical axes of olivine and the mineral foliation and lineation.

Petrostructural studies of olivine in the **plagiodunites** from the Talazhin massif have revealed similar predominant orientations of the mineral both by shape and by internal structure (Fig. 5). The crystal-optical N_g and N_p axes form almost similar petrostructural patterns correlating with the mineral foliation and lineation. The aligned concentration belts of the optical axes are arranged normally to the mineral lineation. Within the belts, there are local maxima of the N_g (6–8%) and N_p (4–6%) axes normal to the mineral foliation. One of the N_g maxima (4%) lies in the mineral foliation and is normal to the mineral lineation. The other local maxima of these axes are oriented at different angles in the foliation. The N_m axes in both samples have a single high-density (10%) maximum each. They are aligned with the lineation and tend to stretch into a belt along the foliation.

Olivine in the **troctolite** from the Talazhin massif also has a predominant optical orientation (Fig. 5) similar in petrostructural patterns to that in the plagiodunites. The petrostructural patterns along the N_g and N_p axes are related to the mineral foliation and lineation. They form aligned concentration belts normal to the lineation, with distinct local maxima on the N_g (6%) and N_p (8%) axes, which are normal to the mineral foliation. The maxima of the N_g axes lie in the foliation normally to the lineation. The rest local maxima of the axes are oriented at different angles to the foliation. The N_m axis has one high-density (10%) maximum aligned with the lineation. One more local maximum of this axis (4%) lies in the foliation.

Invoking literature data (Chernyshov, 2001; Kazakov, 1987), we analyzed the petrostructural patterns of olivine in the plagiodunites and troctolites from the Talazhin intrusion and concluded that the mineral resulted from the magmatic crystallization of melt and subsequent plastic deformations.

At the first stage, optical orientations formed, which were determined by the grain shape and the flow of magmatic liquid (Chernyshov et al., 2004), both isolated crystals and a mixture of cumulus crystals with a minor intercumulose liquid. The maximum of the N_m axes was aligned with the direction of flow (*L*). It lies in the flow plane, and the other two optical axes form orthogonal maxima. The most distinct maximum of the N_p axes was probably oriented normally to the flow plane. This petrostructural pattern of olivine usually forms in the case of a laminar flow of magmatic liquid, accompanied by a weak turbulent rotation of cumulus crystals (Chernyshov et al., 2004).

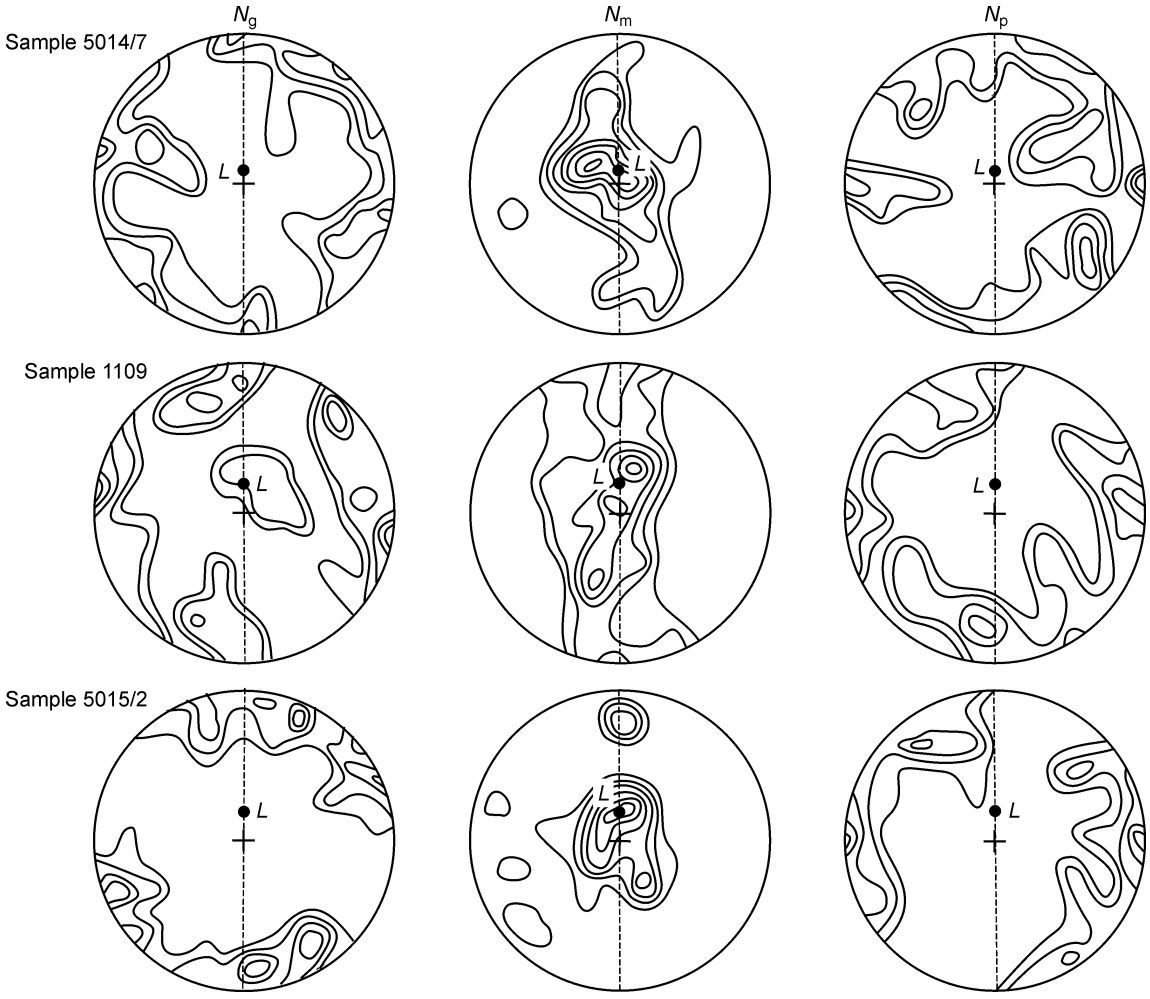

Fig. 5. Diagrams of orientation of the optical-indicatrix axes of olivine in plagiodunites (samples 5014/7 and 1109) and troctolite (sample 5015/2) from the Talazhin massif. Constructed after 50 measurements of the optical indicatrix. Isolines: 1–2–4–6–8–10% per 1% of the Schmidt's net. Projection to the upper hemisphere. Dotted line marks the plane of mineral flattening; *L*, mineral linearity.

At the second stage, when the quantity of crystals in magma increased and they could respond to dynamic loads (Shcherbakov, 1985), the optical orientation of olivine became more complex. Plastic deformations were exhibited as a change of the systems of translation slip in the mineral from moderate- to low-temperature ones: (110)[001] → (100)[001]. The direction of translation slip [001] = N_m was controlled by a plastic flow in the rock (*L*). The directions of translation slip in olivine and plastic flow in the rock, determined by $L = N_m$, were inherited from the direction of the melt motion. Plane (110) is detected from the presence of the N_g and N_p maxima localized at an angle to the mineral foliation, and plane (100), from the presence of a local N_g maximum normal to the foliation. These deformations resulted in aligned concentration belts along the N_g and N_p axes. The petrostructural pattern with N_m maximum established in the plagiodunites forms a belt along the mineral foliation and obviously indicates a superposed plastic deformation as a result of syntectonic recrystallization in completely solidified rocks.

Thus, the petrostructure of the Talazhin olivine seems to have formed under conditions of a laminar flow of magmatic liquid in an intrusion chamber with decreasing temperature, slow deformation, and low external stress rather than under stationary conditions, when isotropic petrostructural patterns form as a result of the gravitational settling of crystals (Chernyshov, 2001). The subsequent superposed dynamic loads led to the complication of petrostructural patterns and the plastic deformation of olivine grains.

Petrochemical features of intrusive rocks

The main petrochemical features of the intrusive rocks of the Talazhin massif are listed in Table 5 and on the variation diagrams in Fig. 6. For comparison, the average compositions of the main types of rocks of the petrographically similar Voices Bay (Naldrett, 2003) and Yoko-Dovyren (Konnikov, 1986) massifs are shown. The most typical petrochemical features of all these massifs are SiO_2 undersaturation, high

Table 5. Chemical composition of the main types of rocks of the Talazhin massif

Component	Plagiodunites						Olivine gabbro	
	8140/1	11695a	8161	4202	5014/7	1093	5003/1	5003/3
SiO_2, wt.%	39.67	40.97	41.99	39.82	40.93	41.26	43.24	43.10
TiO_2	0.21	0.45	0.28	0.25	0.05	0.06	0.13	0.17
Al_2O_3	0.84	6.61	4.05	3.72	6.06	4.92	16.11	15.92
FeO_{tot}	20.37	14.99	13.50	15.94	16.60	15.61	9.18	9.96
MnO	0.16	0.25	0.16	0.26	0.25	0.26	0.13	0.17
MgO	35.97	31.79	37.76	38.66	32.40	35.87	20.48	19.87
CaO	1.67	4.12	1.36	0.32	2.95	1.76	9.30	9.05
Na_2O	0.03	0.11	0.03	0.05	0.67	0.19	1.28	1.35
K_2O	0.06	0.07	0.12	0.09	0.05	0.04	0.14	0.12
P_2O_5	0.02	0.04	0.02	0.09	0.03	0.02	0.02	0.02
Total	99.01	99.41	99.27	99.20	100.00	100.00	100.00	99.73
Component	Troctolites							
	8314/1	25422	8222/1	5011	5013/1	5014	5020	5003/5
SiO_2, wt.%	45.31	43.05	43.02	43.77	45.18	42.89	44.99	47.86
TiO_2	0.90	0.17	0.18	0.04	0.09	0.03	0.06	0.22
Al_2O_3	19.56	11.20	11.01	21.20	26.32	15.92	23.82	24.53
FeO_{tot}	11.46	10.91	12.86	6.35	4.10	9.35	5.44	5.07
MnO	0.17	0.22	0.27	0.08	0.05	0.14	0.07	0.07
MgO	9.80	28.84	27.50	15.72	8.00	21.64	10.13	7.27
CaO	10.75	5.19	4.80	11.37	14.32	8.63	13.36	11.31
Na_2O	1.35	0.08	0.06	1.38	1.82	1.24	1.98	2.97
K_2O	0.15	0.03	0.06	0.07	0.10	0.14	0.12	0.68
P_2O_5	0.03	0.02	0.02	0.02	0.02	0.02	0.02	0.03
Total	99.48	99.71	99.80	100.00	100.00	100.00	100.00	100.00
Component	Anorthosites							
	8313	8316	8311	8314	8315	8311/1	5020/2	5015/1
SiO_2, wt.%	45.15	46.29	45.35	46.96	47.18	47.85	45.80	46.36
TiO_2	0.39	0.57	0.18	0.42	0.42	0.70	0.17	0.15
Al_2O_3	25.35	25.86	24.51	26.18	26.54	23.51	26.75	27.37
FeO_{tot}	6.45	5.76	6.24	5.47	5.35	7.13	4.20	3.32
MnO	0.11	0.10	0.11	0.10	0.09	0.12	0.05	0.05
MgO	9.16	5.99	11.11	6.54	5.89	7.09	6.16	5.38
CaO	12.00	11.85	11.17	12.53	12.22	11.29	14.23	13.91
Na_2O	1.16	1.97	1.01	1.47	1.50	1.85	2.45	2.37
K_2O	0.18	0.41	0.09	0.14	0.59	0.21	0.17	1.07
P_2O_5	0.02	0.04	0.02	0.01	0.02	0.03	0.02	0.02
Total	99.97	98.85	99.80	99.83	99.81	99.78	100.00	100.00

Note. The chemical composition of rocks was determined on a Perkin Elmer atomic-absorption spectrometer at the Institute of Geochemistry, Irkutsk (analyst T.V. Ozhogina).

Mg# (Mg/(Mg + Fe)) and Al/(Al + Ca) values, and low contents of TiO_2, P_2O_5, and K_2O as well as a inverse correlation between the contents of MgO and most of rock-forming oxides, except for FeO_{tot}. The only rocks that do not follow these regularities are “leopard” troctolites, olivine gabbro, and magmatic breccias in a conduit hosting sulfide ores and connecting Voices Bay, the main troctolite massif, with a mantle chamber. Similar petrochemical deviations are also observed in the granophyric gabbro of the Yoko-Dovyren pluton (Fig. 6), which are of hybrid nature

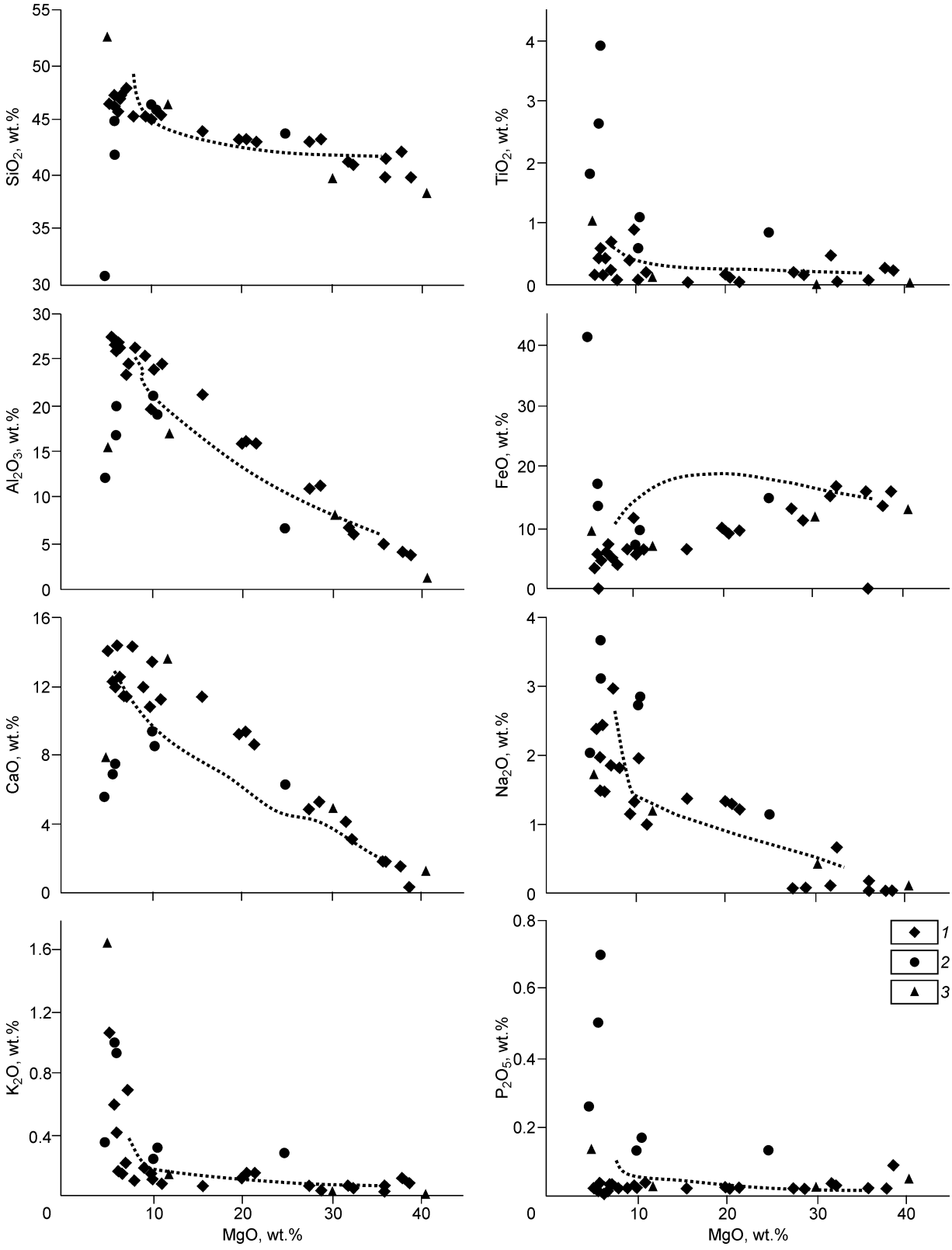

Fig. 6. Rock-forming oxides vs. MgO variation diagrams for rocks of the Talazhin (*1*), Yoko-Dovyren (*2*), and Voices Bay (*3*) massifs. Dotted line is the composition trend of cumulose phases obtained by modeling of the formation of the Talazhin layered intrusion based on the composition of the model parental melt computed by the KOMAGMAT-3.52 program (Ariskin and Barmina, 2000).

(after the data by E.G. Konnikov). These rocks have higher contents of TiO_2, FeO, Na_2O, K_2O, and P_2O_5 and lower contents of SiO_2, Al_2O_3, and CaO than those following from the fractionation trend of the considered intrusive complexes. This trend is, most likely, also related to the hybrid nature of the conduit rocks of the Voices Bay intrusion. It is remarkable that the composition points of the Talazhin massif rocks form a trend that is also slightly typical of hybrid rocks (Fig. 6). This suggests that the Talazhin massif is hardly ore-bearing as compared with the Voices Bay and Yoko-Dovyren massifs hosting Cu–Ni sulfide mineralization.

The geochemical characteristics of the Talazhin intrusion

Nine samples of the Talazhin massif rocks were analyzed for trace elements (Table 6) by ICP MS at the Institute of Geology and Mineralogy, Novosibirsk (Nikolaeva et al., 2008). The results were used to construct their REE patterns normalized to carbonaceous chondrite *C*I (Fig. 7) and trace-element spidergrams normalized to primitive mantle (Fig. 8). These diagrams also include data on the distribution of trace elements in the Voices Bay (Naldrett, 2003) and Yoko-Dovyren (Ariskin et al., 2009) intrusions petrographically similar to the Talazhin massif.

As seen from the Fig. 7, the normalized contents of all REEs in the Talazhin intrusion are close to those in the chondrite, regularly increasing from HREE to LREE. The REE patterns show a distinct positive Eu anomaly, which points to the accumulation of plagioclase under reducing conditions and the fractional crystallization of cotectic Ol–Pl magmas during the formation of the Talazhin intrusion. The REE patterns of the rocks of the Yoko-Dovyren and Voices Bay massifs are similar to those of the Talazhin massif rocks, but the total

Table 6. Contents of trace elements in rocks of the Talazhin massif

Component	Plagiodunite		Serpentinite		Troctolite		Olivine gabbro	Anorthosite	
	5014/7	1093	5020/4	1109	5011	5014	5003/1	5015/1	5020/2
Ga, ppm	7.44	3.81	3.91	3.48	11.47	9.84	11.32	17.30	15.69
Rb	7.31	0.56	1.73	0.76	1.98	5.03	2.83	42.34	4.25
Sr	194.78	47.66	12.09	112.14	458.20	384.15	469.28	863.99	798.59
Y	2.57	0.67	0.89	0.76	0.74	1.51	1.72	1.85	1.29
Zr	13.31	1.96	3.88	2.62	2.62	6.62	4.58	4.97	3.67
Nb	1.06	0.09	0.41	0.13	0.18	0.60	0.20	0.28	0.28
Cs	0.53	0.15	0.23	0.16	0.54	0.99	0.91	1.73	0.61
Ba	68.35	19.41	21.72	10.73	31.20	35.14	47.17	115.33	47.12
La	2.29	0.37	0.55	0.39	0.81	1.11	1.20	1.03	1.09
Ce	4.48	0.74	1.05	0.84	1.56	2.33	2.33	2.05	2.29
Pr	0.58	0.10	0.15	0.11	0.20	0.29	0.30	0.29	0.29
Nd	2.09	0.37	0.57	0.46	0.77	1.27	1.28	1.21	1.26
Sm	0.45	0.09	0.12	0.10	0.14	0.22	0.29	0.29	0.24
Eu	0.15	0.08	0.06	0.08	0.18	0.17	0.24	0.31	0.26
Gd	0.42	0.08	0.12	0.09	0.14	0.28	0.29	0.33	0.24
Tb	0.06	0.01	0.02	0.01	0.02	0.03	0.05	0.04	0.03
Dy	0.38	0.08	0.12	0.09	0.10	0.21	0.26	0.27	0.20
Ho	0.07	0.02	0.03	0.02	0.02	0.04	0.05	0.05	0.04
Er	0.21	0.05	0.07	0.07	0.05	0.11	0.14	0.13	0.11
Tm	0.03	0.01	0.01	0.01	0.01	0.02	0.02	0.02	0.02
Yb	0.21	0.07	0.09	0.08	0.06	0.10	0.12	0.12	0.09
Lu	0.03	0.01	0.02	0.01	0.01	0.01	0.02	0.02	0.01
Hf	0.29	0.04	0.08	0.07	0.06	0.13	0.13	0.13	0.08
Ta	0.13	0.02	0.08	0.03	0.02	0.04	0.04	0.04	0.03
W	0.50	0.28	0.19	0.13	0.22	0.29	0.22	0.28	0.49
Th	0.60	0.03	0.12	0.03	0.09	0.26	0.06	0.06	0.09
U	0.15	0.03	0.13	0.02	0.03	0.07	0.03	0.02	0.04

Note. Analyses were carried out on an ELEMENT (Finnigan Mat) mass spectrometer at the Analytical Center of the Institute of Geology and Mineralogy, Novosibirsk (analyst S.V. Palesskii).

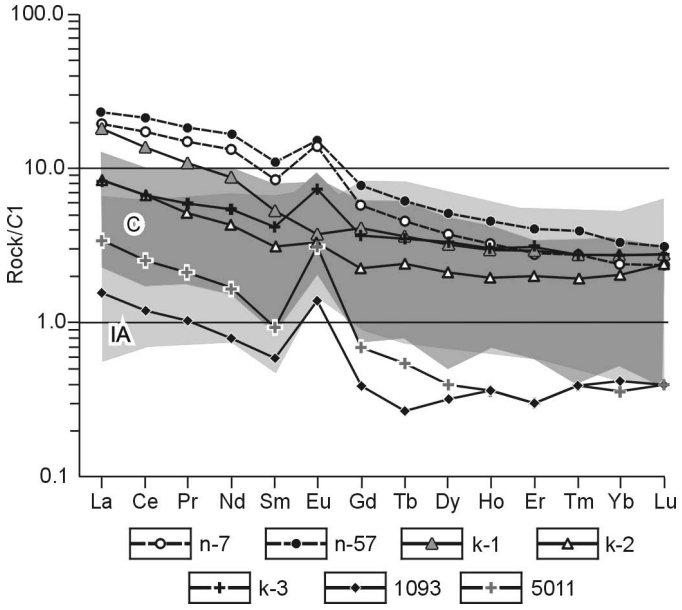

Fig. 7. Chondrite *C*I-normalized (Anders and Grevesse, 1989) REE patterns of rocks of the Talazhin (samples 1093 and 5011), Yoko-Dovyren (samples k-1, k-2, and k-3), and Voices Bay (samples p-7 and p-57) massifs. For comparison, the patterns of layered peridotite–gabbro massifs of island-arc (IA) and collision (C) stages are given.

normalized content of these elements is almost ten times higher. A specific feature of the LREE distribution in the rocks of all these massifs is that the content of HREE changes much less than that of LREE during the differentiation of magma from plagiodunites to gabbroids.

Comparison of the trace-element patterns of the considered intrusive complexes (Fig. 8) shows their great geochemical similarity. The Voices Bay, Yoko-Dovyren, and Talazhin intrusions are strongly enriched in Ba, Pb, and Sr and are depleted in Th, U, Nb, Ta, and Ti relative to the primitive mantle. The Talazhin intrusion is also significantly depleted in HREE (Gd, Dy, Er, Yb, Lu) as compared with the Voices Bay and Yoko-Dovyren massifs. This probably points to the presence of garnet in the rocks of the mantle substratum that produced the parental magma for the intrusion. The high normative contents of typical crustal elements (Ba, Sr, Pb) in the rocks of all considered massifs might be due to the contamination of parental melts with continental crustal material. For the Yoko-Dovyren and Voices Bay intrusions, the interaction of magma with crustal rocks was proved by isotope-geochemical data (Konnikov, 1986; Naldrett, 2003). The signs of these processes in the Talazhin complex might point to its ore potential.

Results of numerical modeling

Using the KOMAGMAT-3.52 program, modeling of fractional crystallization was performed for the main intrusive rock varieties of the Talazhin massif (Ariskin and Barmina, 2000). The presence of iron oxides and water-containing phases (amphibole) in the rocks indicates that the oxygen fugacity during crystallization probably corresponded to the QFM buffer (quartz–fayalite–magnetite). Geological observations (the presence of hornfels xenoliths on the massif periphery) and petrographic data (the presence of minor late-magmatic amphibole (<5%) in the rocks) show that the parental melt crystallized during the formation of the layered series at a lithostatic pressure no higher than 3 kbar, with the initial water content in the melt not exceeding 0.5 wt.%. Based on these

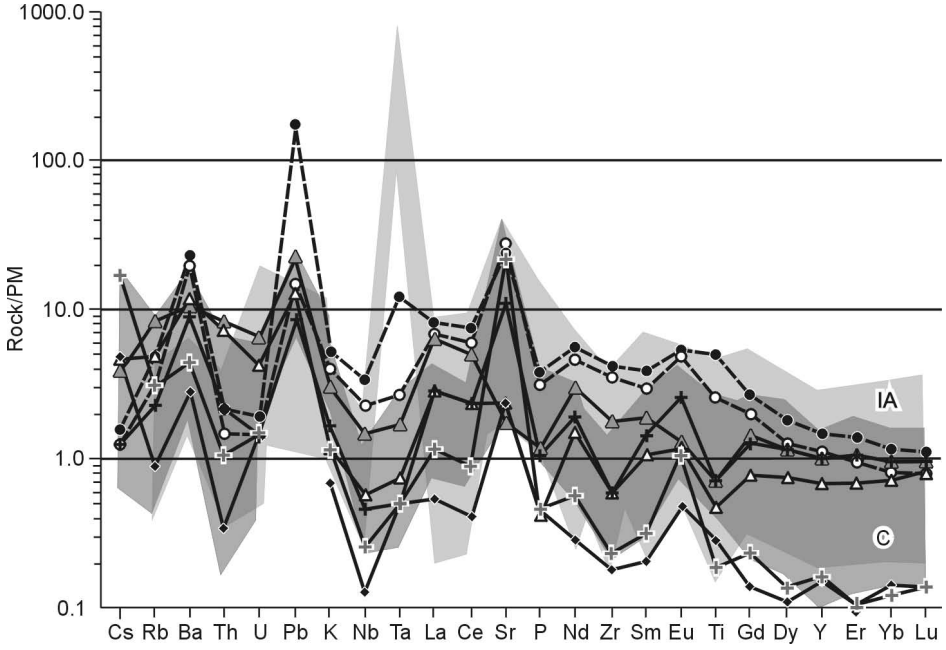

Fig. 8. Primitive-mantle-normalized (Sun and McDonough, 1989) spidergrams of the most abundant trace elements in rocks of the Talazhin, Yoko-Dovyren, and Voices Bay massifs. Designations follow Fig. 7.

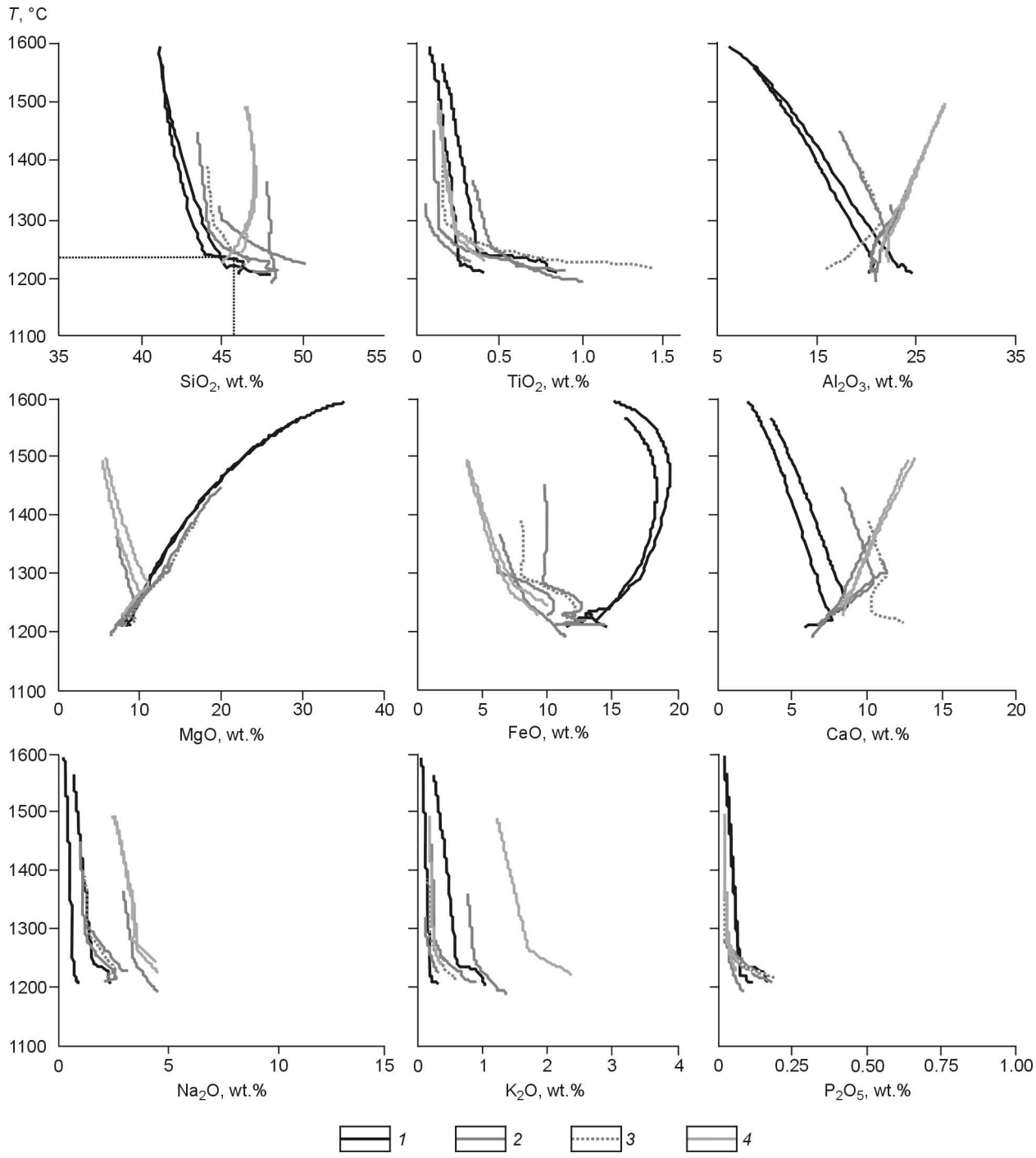

Fig. 9. Equilibrium crystallization curves modeled using the KOMAGMAT-3.52 program (Ariskin and Barmina, 2000) for the main intrusive rock varieties of the Talazhin massif. *1*, plagiodunite; *2*, troctolite; *3*, olivine gabbro; *4*, anorthosite.

data, computations were made in the regime of formation of layered intrusion with the following system parameters: 1–2 kbar, QFM buffer, water content of 0–0.5%, and melt crystallization step of 1 mol.%. The melt crystallization trends were computed up to 66–90% crystals (34–10% residual liquid) depending on the rock composition. According to the results obtained, the equilibrium crystallization of the Talanzhin intrusion melt proceeded in the sequence Ol → Ol + Pl → Ol + Pl + Cpx.

The compositions of cumulose phases were obtained by modeling the formation of layered intrusion, based on the composition of the model parental melt computed by the KOMAGMAT-3.52 program. The composition trend is similar to that of the massif rocks of the layered series on the variation diagrams (Fig. 6), and the factual and computed compositions of minerals in these rocks agree with each other, which indicates that the accepted parameters of the model system are close to those of the natural system.

Figure 9 presents results of computation for eight samples of the Talazhin massif rocks, which reflect the temperature–composition evolution of residual (intercumulose) melts in terms of the contents of nine rock-forming oxides. The computed trends for all components are proximal to each other and intersect in the temperature range 1240–1260 ºC, forming compact clusters near the olivine–plagioclase cotectic curve. These intersections are the most distinct on the temperature vs SiO_2, Al_2O_3, MgO, CaO, and P_2O_5 diagrams. Thus, the average value of 1250 ºC can be taken as the probable temperature of the parental magma for the Talazhin intrusion. The composition of this melt at 1250 ºC can be estimated from Fig. 9 (wt.%): SiO_2—46, TiO_2—0.35, Al_2O_3—21.5, FeO_{tot}—10, MgO—10, CaO—8, Na_2O—2.5, K_2O—0.5, and P_2O_5—0.07.

The estimated composition of the parental magma corresponds to low-Ti high-alumina olivine–basalt melt. This is also evidenced from the petrochemical features of the Talazhin massif rocks (low Ti contents, low Fe/(Fe + Mg) ratios, depletion in alkalies (especially K), and enrichment in Mg, Ni, and Cr), which are typical of rocks of the tholeiitic petrochemical series (Bogatikov et al., 2010).

Discussion and conclusions

Thus, the data obtained show that the Talazhin intrusion is a rhythmically layered plagiodunite–troctolite–anorthosite–gabbro massif. In a series of features (mineralogical and petrographic (high Fe/(Fe + Mg) value of olivine, high basicity of plagioclase, kind of rock layering) and geochemical (HREE depletion, LREE enrichment, negative Ta and Hf anomalies)) it is similar to high-alumina island-arc massifs of Vendian–Cambrian age (Fig. 7) (Izokh et al., 1998). Still greater similarity is observed between the Talazhin massif and Ordovician collisional layered peridotite–gabbro massifs, in particular, the Mazhalyk massif of the Central Asian Fold Belt in southeastern Tuva (Borodina et al., 2004), the Bulka massif in northeastern West Sayan (Borodina et al., 2011), and Lukinda massif of the West Stanovoy terrane on the southern periphery of the North Asian craton (Buchko, 2010).

The similarity of the petrological and geochemical characteristics of rocks of the layered peridotite–gabbro massifs formed at the collision and island-arc stages is due to the generation of their parental melts as a result of the partial melting of the same depleted suprasubductional mantle source compositionally corresponding to garnet lherzolite (Borodina et al., 2004).

The Talazhin massif obviously belongs to a Riphean plagiodunite–troctolite–anorthosite–gabbro formation regarded as a potential Riphean source of PGE–Cu–Ni mineralization (Kislov, 2009). Our investigations show that the Talazhin massif is similar in petrographic composition and petro- and geochemical features to the Yoko-Dovyren and Voices Bay layered massifs hosting Cu–Ni–PGE sulfide mineralization and deposits. This permits us to consider it promising for such mineralization. The ore potential of the massif is evidenced by the high contents of Ni (0.2%), Cu (0.3%), and PGE (up to 380 ppm) in the rocks (unpublished data by A.G. Ekhanin, A.N. Smagin, and A.V. Renzhin).

We thank A.A. Ariskin, Professor of Moscow State University and a leading researcher of the Vernadsky Institute of Geochemistry and Analytical Chemistry, Moscow, for consultations on the aspects of parental-melt modeling using the KOMAGMAT program.

References

Anders, E., Grevesse, N., 1989. Abundances of the elements: meteoritic and solar. Geochim. Cosmochim. Acta 53, 197–214.

Ariskin, A.A., Barmina, G.S., 2000. Modeling of Phase Equilibria during Crystallization of Basaltic Magmas [in Russian]. Nauka, Moscow.

Ariskin, A.A., Konnikov, E.G., Kislov, E.V., 2003. Modeling of equilibrium crystallization of ultramafic rocks as applied to the problem of formation of the phase layering of the Dovyren pluton (northern Baikal area). Geokhimiya, No. 2,131–155.

Ariskin, A.A., Konnikov, E.G., Danyushevsky, L.V., Kislov, E.V., Nikolaev, G.S., Orsoev, D.A., Barmina, G.S., Bychkov, K.A., 2009. The Dovyren intrusive complex: problems of petrology and nickel–sulfide mineralization. Geokhimiya, No. 5, 451–480.

Bogatikov, O.A., Kovalenko, V.I., Sharkov, E.V., 2010. The Earth's Magmatism, Tectonics, and Geodynamics [in Russian]. Nauka, Moscow.

Borodina, E.V., Egorova, V.V., Izokh, A.E., 2004. Petrology of Ordovician collision-related layered peridotite–gabbro intrusions (exemplified by the Mazhalyk intrusion, Southeastern Tuva). Geologiya i Geofizika (Russian Geology and Geophysics) 45 (9), 1074–1091 (1025–1042).

Borodina, E.V., Izokh, A.E., Mongush, A.A., 2011. The Bulka peridotite–gabbro intrusion (West Sayan), a syncollisional type of layered intrusions. Russian Geology and Geophysics (Geologiya i Geofizika) 52 (3), 307–319 (393–408).

Buchko, I.V., 2010. The Stages of Ultramafic–Mafic and Gabbro–Anorthosite Magmatism on the Southeastern Framing of the North Asian Craton. ScD Thesis [in Russian]. IGiP DVO RAN, Vladivostok.

Chernyshov, A.I., 2001. Ultramafic Rocks: Plastic Flow, Structural and Petrostructural Inhomogeneities [in Russian]. Charodei, Tomsk.

Chernyshov, A.I., Nozhkin, A.D., Stupakov, S.I., Balykin, P.A., Kuzovatov, N.I., Reznikov, I.G., Tret'yakov, N.A., Prokhorova, V.A., 2004. The Kingash ultramafic–mafic massif: geologic position, internal structure, petrographic composition, and petrostructural analysis of ultramafic rocks (East Sayan), in: Platinum of Russia. Geoinformmark, Moscow, Vol. 5, pp. 152–175.

Chernyshov, A.I., Nozhkin, A.D., Mishenina, M.A., 2010. Petrochemical typification of the ultramafic rocks of the Kan Block (East Sayan). Geokhimiya, No. 2, 1–25.

Glazunov, O.M., 1995. The Kingash massif, in: The Platinum Potential of Ultrabasic–Basic Complexes in Southern Siberia [in Russian]. Izd. SO RAN, NITs OIGGM SO RAN, Novosibirsk, pp. 53–63.

Glazunov, O.M., Bognibov, V.I., Ekhanin, A.G., 2003. The Kingash PGE–Cu–Ni Deposit [in Russian]. Izd. IGTU, Irkutsk.

Izokh, A.E., Polyakov, G.V., Gibsher, A.S., Balykin, P.A., Zhuravlev, D.Z., Parkhomenko, V.A., 1998. High-alumina stratified gabbroids of the Central-Asian fold belt: geochemistry, Sm–Nd isotopic age, and geodynamic conditions of formation. Geologiya i Geofizika (Russian Geology and Geophysics) 39 (11), 1565–1577 (1565–1577).

Kazakov, A.I., 1987. Dynamic Analysis of Microstructural Orientations of Minerals [in Russian]. Nauka, Leningrad.

Kislov, E.V., 1998. The Yoko-Dovyren Layered Massif [in Russian]. Izd. BNTs SO RAN, Ulan Ude.

Kislov, E.V., 2009. The Riphean PGE–Cu–Ni metallogenic epoch: ore formation factors, in: Petrology of Igneous and Metamorphic Complexes [in Russian]. TsNTI, Tomsk, Issue 7, pp. 328–338.

Konnikov, E.G., 1986. Differentiated Precambrian Ultrabasic–Basic Complexes in Transbaikalia [in Russian]. Nauka, Novosibirsk.

Kornev, T.Ya., Ekhanin, A.G., Romanov, A.P., Knyazev, V.N., Sharifulin, S.K., 2003. The Kan Greenstone Belt and Its Metallogeny (East Sayan) [in Russian]. KNIIGiMS, Krasnoyarsk.

Leake, B.E., Woolley, A.R., Arps, C.E.-S., Birch, W.D., Gilbert, M.Ch., Grice, J.D., Hawthorne, F.C., Kato, A., Kisch, H.J., Krivovichev, V.G., Linthout, K., Laird, J., Mandarino, J.A., Maresch, W.V., Nickel, E.H., Rock, N.M.S., Schumacher, J.C., Smith, D.C., Stephenson, N.C.-N., Ungaretti, L., Whittaker, E.J.-W., 1997. Nomenclature of amphiboles: report of the Subcommittee on Amphiboles of the International Mineralogical Association, Commission on New Minerals and Mineral Names. Can. Mineral. 35, 219–246.

Naldrett, A.J., 2003. Magmatic Sulfide Deposits of Copper–Nickel and Platinum Metal Ores [in Russian]. Izd. SPb. Univer., St. Petersburg.

Nikolaeva, I.V., Palessky, S.V., Koz'menko, O.A., Anoshin, G.N., 2008. ICP MS determination of rare-earth and high-field strength elements in standard geologic samples. Geokhimiya, No. 10, 1085–1091.

Shcherbakov, S.A., 1985. Microstructural analysis of the ultrabasic rocks of the Pacific and Indian Oceans. Izd. Akad. Nauk. Ser. Geol., No. 3, 54–56.

Sokolov, G.A., 1948. Urals chromites: composition, crystallization conditions, and distribution regularities. Series of ore deposits (No. 12). Trudy IGN AN SSSR, Issue 97.

Sun, S.S., McDonough, W.F., 1989. Chemical and isotopic systematics of oceanic basalts: implications for mantle composition and processes, in: Saunders, A.D., Norry, M.J. (Eds.), Magmatism in the Oceanic Basins. Geol. Soc. Spec. Publ., No. 42, 313–345.

Editorial responsibility: A.E. Izokh